

AnisEulerSC: A MATLAB program combined with MTEX for modeling the anisotropic seismic properties of a polycrystalline aggregate with microcracks using self-consistent approximation

Eunyoung Kim^a, YoungHee Kim^{a,*}, David Mainprice^b

^a School of Earth and Environmental Sciences, Seoul National University, Seoul, 08826, Republic of Korea

^b Géosciences Montpellier UMR CNRS 5243, Bâtiment 22, CC 060, Université de Montpellier, Place Eugène Bataillon, 34095, MONTPELLIER Cedex 05, France



ARTICLE INFO

Keywords:

Rock microstructure
Crack orientation
Seismic anisotropy
Self-consistent approximation
MTEX
MATLAB

ABSTRACT

Seismic anisotropy of polycrystalline materials depends on the characteristics of microcracks as well as the crystallographic orientations of minerals. Here, we present a MATLAB-based software, AnisEulerSC (Anisotropy from Euler angles using Self-Consistent approximation), for modeling the anisotropic seismic properties of a polycrystalline aggregate with microcracks using the self-consistent approximation. In this program, several commands of MTEX (a MATLAB toolbox for texture analysis) are utilized to analyze constituent components of a rock sample based on experimental measurement data (e.g., electron backscatter diffraction) and to calculate and visualize seismic wave velocities and polarizations. We provide several examples of SC modeling to explore the effects of grain shapes on a polycrystalline aggregate and the effects of crack shapes and orientations on the anisotropic seismic properties of a polycrystalline aggregate.

1. Introduction

Characteristics of microcracks strongly impact the seismic properties of rocks and provide important information about the tectonic history of igneous and metamorphic rocks (Simmons and Richter, 1976) as well as sedimentary rocks (Sayers and Munster, 1991). A microcrack, defined as an opening occurring in rock, has a width-to-length ratio (or aspect ratio) less than 10^{-2} (typically 10^{-3} to 10^{-5}) and a length on the order of 100 μm or less (Simmons and Richter, 1976). Because the preferred orientation of microcracks influences the seismic anisotropy of rock along with the crystallographic preferred orientation (CPO), shape preferred orientation (SPO), and thin layers of isotropic materials with different properties (Cyprych et al., 2017; Kern et al., 2008), it is important to consider the shapes and distributions of microcracks to predict seismic velocities and anisotropy using theoretical methods.

Budiansky (1965) and Hill (1965) introduced the self-consistent (SC) approximation, originally proposed for crystal aggregates by Hershey (1954) and Kröner (1958), which considers the interaction between inclusions when estimating the elastic moduli of heterogeneous composites. To take into account the influence of crack interaction, Budiansky and O'Connell (1976) used the SC scheme to calculate the elastic properties of isotropic solids with a random distribution of

ellipsoidal cracks. The SC approximation has also been used to solve the bulk and shear modulus for a two-phase composite (e.g., Wu, 1966) and for a multiphase material composed of N number of inclusion phases (e.g., Berryman, 1995). Eshelby (1957) theory, which is used to solve problems related to the elastic field of an ellipsoidal inclusion in an infinite medium, is a fundamental element of SC approximation for anisotropic background media (Kinoshita and Mura, 1971).

Experiments on rock samples showed that seismic anisotropy in the crust and mantle is caused by CPO, SPO, and/or oriented cracks with ellipsoidal shapes (e.g., Burlini and Kunze, 2000; Kern et al., 2008; Wenk et al., 2012). In a granite matrix with aligned ellipsoidal fluid-filled cracks, the P-wave velocity is lower for propagation along the symmetric axis (Anderson et al., 1974). Anderson et al. (1974) also showed that P-wave anisotropy increases as the pore fluid bulk modulus decreases. Because the seismic velocities of rocks depend strongly on the characteristics of cracks (Simmons and Richter, 1976), it is important to investigate the effects of the shapes and orientations of cracks on seismic anisotropy (e.g., Morales et al., 2018). In the problem of the elastic moduli of a cracked solid, previous studies assumed dilute crack concentrations, which means no interactions between cracks (e.g., Walsh, 1965a, 1965b; Anderson et al., 1974; Stiller et al., 1977). However, it is necessary to consider the elastic interaction among neighboring cracks

* Corresponding author.

E-mail addresses: brilliant@snu.ac.kr (E. Kim), younghkim@snu.ac.kr (Y. Kim), david.mainprice@umontpellier.fr (D. Mainprice).

as well as mineral grains at higher concentrations of cracks. Because the SC method allows consideration of the interactions between inclusions (Berge et al., 1993), as well as CPO, SPO, and microcrack effects, the SC approximation is appropriate for calculating the elastic properties of a polycrystalline aggregate with microcracks.

In this paper, we present a method that predicts the anisotropic seismic properties of a polycrystalline aggregate with microcracks using the SC approximation. For this modeling, we developed a MATLAB-based software, entitled “AnisEulerSC (Anisotropy from Euler angles using Self-Consistent approximation)”, which was originally written in FORTRAN code (Mainprice, 1990, 1997), to calculate the SC scheme using volume fractions, single-crystal elastic stiffness tensors, and CPO and SPO of constituent phases. For input data on the crystallographic texture and microstructure of rock samples, this program utilizes the MTEX (MATLAB toolbox for texture analysis; Hielscher and Schaeben, 2008) to import, analyze, and plot experimental data. We describe the SC approximation in Section 2, introduce the AnisEulerSC program in Section 3, and provide several examples of SC modeling in Section 4.

2. Self-consistent (SC) approximation

For the prediction of effective elastic properties of complex aggregates, the SC formula is symmetrical in the constituents because each component is assumed to be an inclusion without any host material (Berryman and Berge, 1993). The basis for the SC approximation is the Eshelby (1957) solution, which describes the elastic stress disturbed by the existence of an ellipsoidal inclusion in an infinite isotropic medium (e.g., Mainprice, 1997, 2007). Eshelby (1957) solved the elastic field using a procedure of imaginary cutting, straining, and welding operations. As a result, the stress in the surrounding matrix is zero, whereas it is a known constant value in the inclusion (Eshelby, 1957). This stress-free transformation strain is referred to as the eigenstrain, which is a term given by Mura (1987) to nonelastic strains such as thermal expansion, phase transformation, initial strains, plastic strains, and misfit strains.

For an anisotropic background medium, the uniform strain tensor inside the inclusion (ϵ_{ij}), given by Kinoshita and Mura (1971), is described as follows:

$$\epsilon_{ij} = \frac{1}{2} (G_{ikjl} + G_{jkl}) C_{klmn} \epsilon_{mn}^* \quad (1)$$

where G_{ikjl} is the tensor Green's function associated with displacement due to a unit force applied in a given direction, C_{klmn} is the elastic stiffness tensor of the background medium, and ϵ_{mn}^* is the eigenstrain tensor. The symmetrical tensor Green's function G_{ikjl} is evaluated using the solution given by Mura (1987):

$$G_{ikjl} = \frac{1}{4\pi} \int_0^\pi \sin \theta d\theta \int_0^{2\pi} \left(K_{ij}^{-1}(x) x_k x_l \right) d\varphi \quad (2)$$

where θ and φ are the spherical coordinates for the definition of vector x with respect to the principal axes of the ellipsoidal inclusion. $K_{ij}^{-1}(x)$ is the inverse of the Christoffel stiffness tensor for a direction (x), which is defined as $K_{ij}(x) = C_{ipjq} x_p x_q$. Here $x_1 = \sin \theta \cos \varphi / a_1$, $x_2 = \sin \theta \sin \varphi / a_2$, and $x_3 = \cos \theta / a_3$ for the semi-axes a_1 , a_2 , and a_3 of the ellipsoidal inclusion, respectively. Following Mainprice's (1997) scheme, the Fourier transform of G_{ikjl} is used for numerical calculation of the tensor Green's function. We use the scheme of Willis (1977) in which the strain ratio (A_i) between strains inside and outside the inclusion in the background medium is defined as

$$A_i = [I + G(C_i - C^{SCA})]^{-1}, \quad (3)$$

where I is the symmetrical fourth-rank unit tensor $I_{ijkl} = 1/2(\delta_{ik}\delta_{jl} + \delta_{il}\delta_{jk})$, δ_{ik} is the Kronecker delta, and C_i is the elastic stiffness tensor of

the i th inclusion. The effective elastic stiffness tensor (C^{SCA}) is related to the averaged strain ϵ^{SCA} and stress σ^{SCA} tensors based on the volume averaged Hooke's law:

$$\langle \epsilon^{SCA} \rangle = \sum_{i=1}^{i=n} V_i A_i \quad (4)$$

$$\langle \sigma^{SCA} \rangle = \sum_{i=1}^{i=n} V_i C_i A_i \quad (5)$$

$$C^{SCA} = \langle \sigma^{SCA} \rangle \langle \epsilon^{SCA} \rangle^{-1} \quad (6)$$

where V_i is the volume fraction of the i th inclusion. Because C^{SCA} occurs on both sides of the equation (see Eqs. (3)–(6)), the solution has to be found by iteration (Mainprice, 1997).

3. AnisEulerSC

We present a MATLAB-based program, AnisEulerSC, for modeling the anisotropic seismic properties of a polycrystalline aggregate with microcracks using the SC approximation. Our program utilizes several commands of MTEX (Hielscher and Schaeben, 2008; Mainprice et al., 2011) to calculate and visualize the seismic velocities and anisotropy. The SC scheme in AnisEulerSC, based on the FORTRAN code developed by Mainprice (1990, 1997), considers the crystallographic textures of minerals and microstructural information (e.g., grain shapes and orientations, crack porosity, and geometry). We also present AnisEulerSC-Inputs, a MATLAB-based program composed of graphical user interfaces (GUIs), developed for generating the input parameters as a MATLAB data file (*.mat) to run the AnisEulerSC program (Figs. 1–3). Using AnisEulerSC-Inputs, the composition of a polycrystalline aggregate (Fig. 2), the volume fractions of constituent phases (Fig. 2), and the shapes and orientations of grains (Fig. 3) can be specified. AnisEulerSC-Inputs was designed using MATLAB (R2019a) App Designer in Mac OS X. The AnisEulerSC-Inputs and AnisEulerSC programs run in the MATLAB version after R2016b in Windows or UNIX OS.

For the AnisEulerSC program, MTEX commands ([http://mTEX-toolbox.github.io/](http://mtex-toolbox.github.io/)) are used to import, analyze, and plot the rock sample data of mineral texture and microstructure from experimental measurements such as electron backscatter diffraction (EBSD). The MTEX commands are used to extract information on the volume (or area) fractions and crystal properties of constituent minerals as well as the grain shapes and orientations of minerals. This information is used to specify the mineral properties in AnisEulerSC-Inputs. The output file generated from AnisEulerSC-Inputs contains all of the input parameters required to run the AnisEulerSC program. The Voigt (1928), Reuss (1929), and Voigt-Reuss-Hill (VRH; Hill, 1952) averages (described in Appendix B of the user guide) are automatically calculated in the AnisEulerSC program, and one of them can be used as an initial value of an SC aggregate. The anisotropic seismic velocities of the final SC model are also automatically plotted using the MTEX commands in the AnisEulerSC program. We describe details about how to use the AnisEulerSC-Inputs and AnisEulerSC programs in the user guide. We also provide example data and demo scripts for users to reproduce examples. The AnisEulerSC program enables users to align ellipsoidal grains with an arbitrary angle to the specimen reference frame. Thus, the effects of aligned cracks on the anisotropic seismic velocities of rocks can be explored with various shapes and orientations of cracks.

4. Examples

For cracked materials, the effects of cracks on the seismic properties of a polycrystalline aggregate can be explored using the AnisEulerSC program, because it is possible to specify various shapes and orientations of cracks. In Section 4.1, we present an example for SC modeling of the

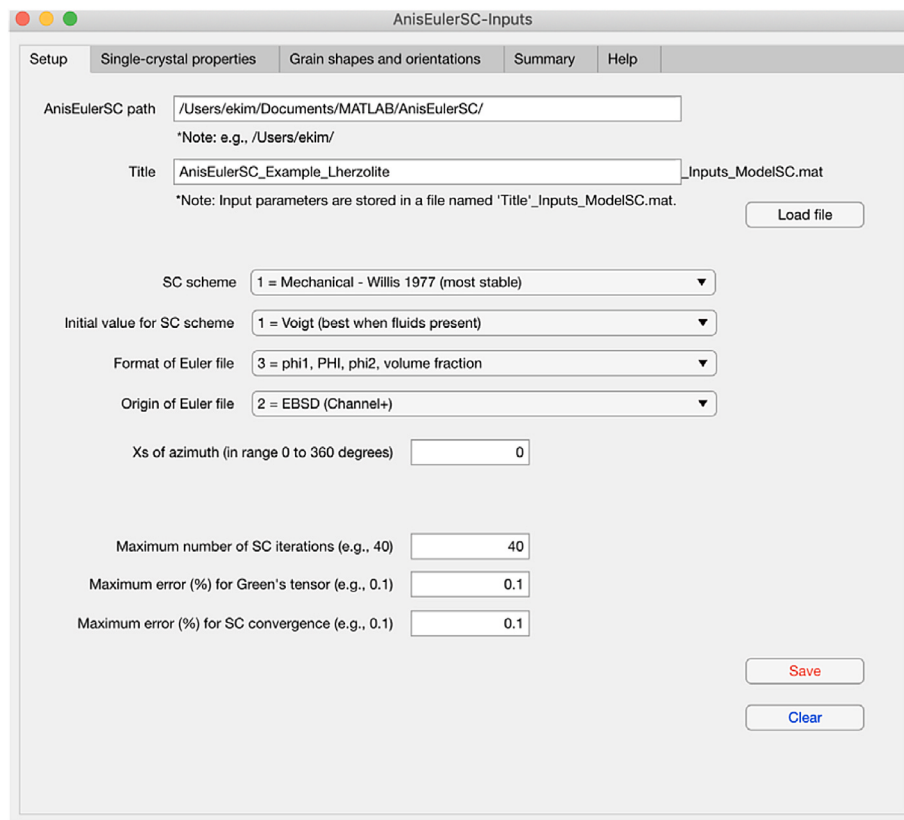


Fig. 1. Setup tab of AnisEulerSC-Inputs, a MATLAB-based program composed of graphical user interfaces (GUIs).

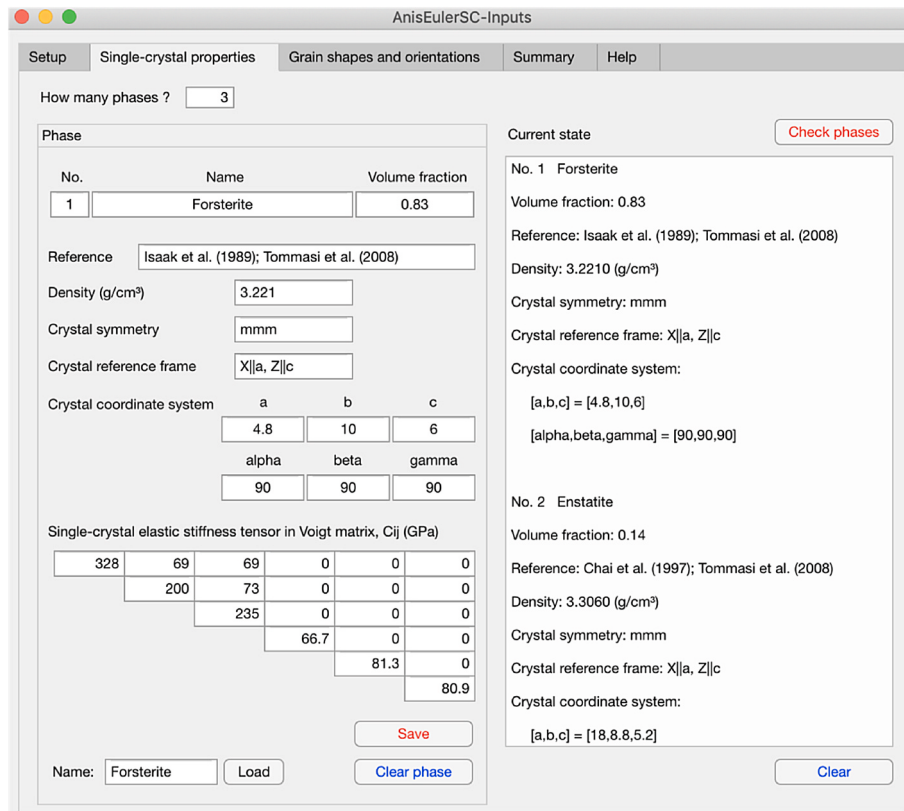


Fig. 2. Single-crystal properties tab of AnisEulerSC-Inputs. For the phase of forsterite, all input data are specified, saved and checked on the 'Current state' screen.

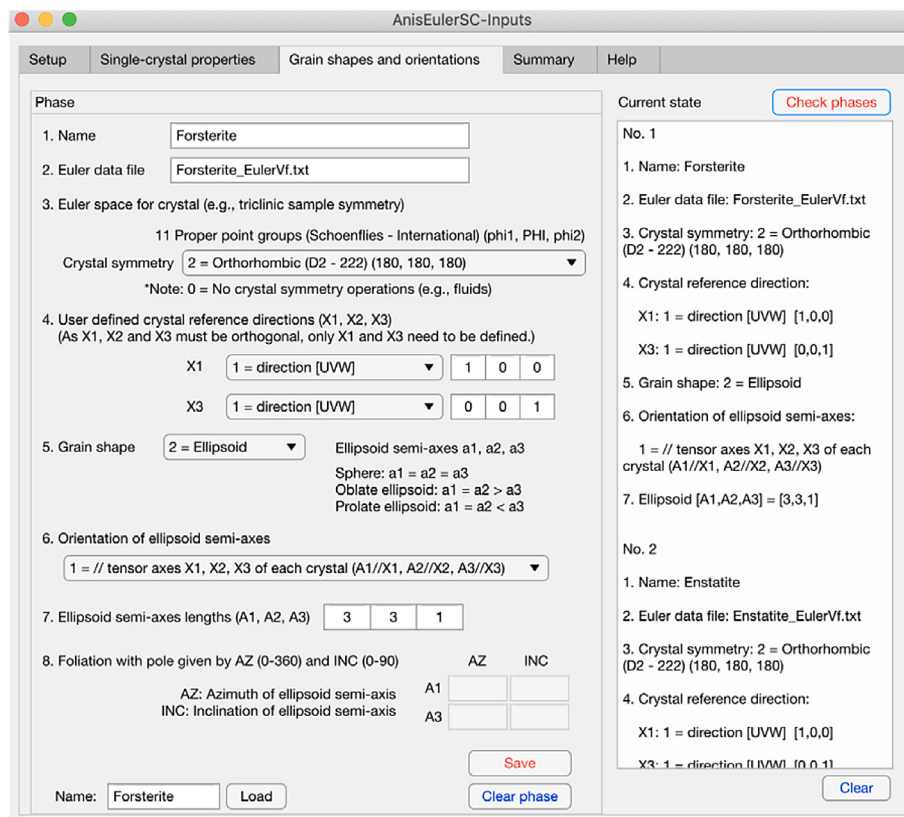


Fig. 3. Grain shapes and orientations tab of AnisEulerSC-Inputs. For the phase of forsterite, all input data are specified, saved and checked on the ‘Current state’ screen.

anisotropic seismic velocities of a polyphase aggregate. In Section 4.2, we present several examples of SC modeling to explore the effects of crack shapes and orientations on the anisotropic seismic properties of rocks. In these sections, we simply explain how to use the programs and how to plot the figures using the step-by-step based process. We describe more details in the user guide and provide example data and demo scripts for the users to reproduce examples.

4.1. SC modeling of anisotropic seismic properties of a polyphase aggregate

We consider a polyphase aggregate composed of forsterite, enstatite, and diopside. For experimentally measured texture and microstructure information, we use the EBSD data of a lherzolite sample, one of the samples from the Tok volcanic field in SE Siberia (Tommasi et al., 2008). Because these samples are spinel peridotite xenoliths related with the shallow lithospheric mantle, Tommasi et al. (2008) performed microstructure analyses to measure the crystallographic orientation to understand how geophysical and geochemical processes such as deformation, static recrystallization, and metasomatism are related to the evolution of the shallow lithospheric mantle.

4.1.1. Step 1: EBSD data analyses

We first analyze the mineral properties of a lherzolite sample by importing the EBSD data into the MTEX. The analyzed properties are used to specify the mineral composition, volume fraction, crystal symmetry, crystal reference frame, crystal orientation, and shape and orientation of grains in the AnisEulerSC-Inputs program. We consider only the indexed phases to make a polycrystalline aggregate composed of forsterite, enstatite, and diopside, because the elastic properties of unindexed phases are unknown. We describe how a single-crystal elastic stiffness tensor is defined by the crystal reference frame and crystal

orientation in terms of the specimen reference frame in Appendix A of the user guide.

To understand the seismic properties of constituent minerals, we calculate and plot the single-crystal seismic velocities of forsterite, enstatite, and diopside (Fig. 4). Based on the Christoffel (1877) equation (described in Appendix B2 of the user guide), the phase velocities and polarizations of the P-wave (V_p) and fast (V_{s1}) and slow (V_{s2}) S-waves of each mineral are calculated and plotted using the MTEX commands (Fig. 4). The single-crystal elastic stiffness tensor, crystal symmetry, and density of forsterite, enstatite, and diopside are described in Figures U3, U5, and U7 of the user guide. We provide a demo script for calculating and plotting the single-crystal seismic velocities (e.g., forsterite; see Demo_of_Crystal_Multi_seismic_plot_MTEX53_EK3_Forsterite.m) for users to reproduce the figures.

To calculate the average elastic properties of a polyphase aggregate, the orientation distribution function of each mineral is needed together with the single-crystal elastic stiffness tensor. Because the AnisEulerSC program requires Euler angles and volume fractions of grains, we extract Euler data from EBSD data using the MTEX commands. We provide a demo script for extracting the grain properties from EBSD data (e.g., lherzolite; see Demo_MTEX_Flexible_Data_Export_Lherzolite.m). The demo script generates Euler data files (*.txt), which are required to run the AnisEulerSC program, that contain Euler angles and area fractions of grains for each mineral. The demo script also plots the EBSD maps as well as the distributions of grain shapes and orientations. Fig. 5 is an EBSD map in which yellow ellipsoids are fitted to the grains of forsterite. The distribution of aspect ratio (long a-axis divided by short b-axis) is plotted against the angle of the long axis to the specimen X-axis (ω) (Fig. 6a–c). Polar histograms are also plotted for the angle of the specimen X-axis at 0° to the long axis of grains (Fig. 6d–f).

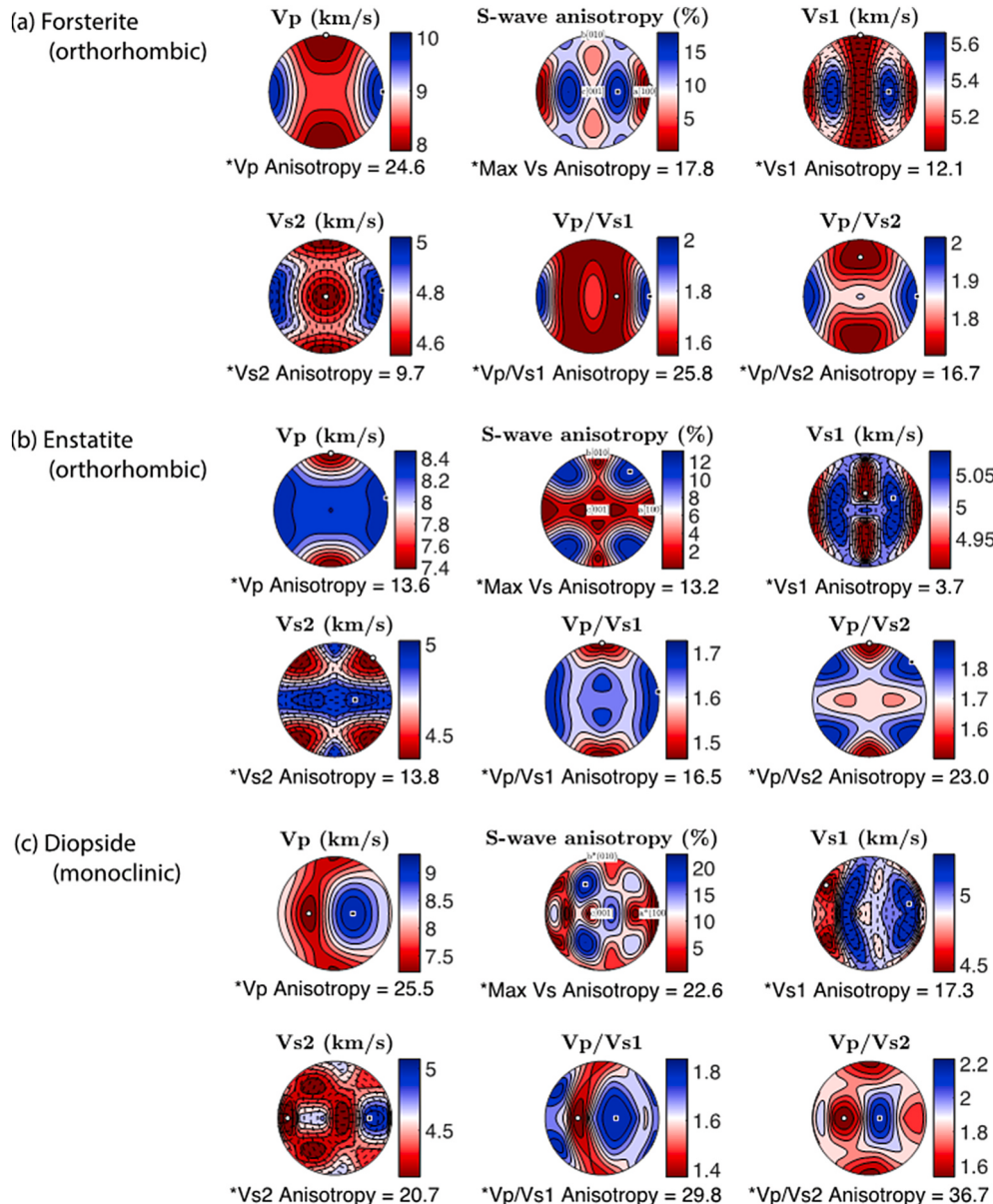


Fig. 4. Multi-plots of single-crystal seismic velocities for (a) forsterite (Isaak et al., 1989; Tommasi et al., 2008), (b) enstatite (Chai et al., 1997; Tommasi et al., 2008), and (c) diopside (Isaak et al., 2006; Tommasi et al., 2008). For each mineral, P-wave velocity (V_p , km/s), S-wave anisotropy (%), fast (V_{s1} , km/s) and slow (V_{s2} , km/s) S-wave velocities, and V_p/V_{s1} and V_p/V_{s2} are calculated based on the Christoffel (1877) equation for an anisotropic elastic medium. The anisotropy of each elastic velocity is shown as a percentage. All seismic velocities and anisotropies are calculated and plotted using the MTEX commands.

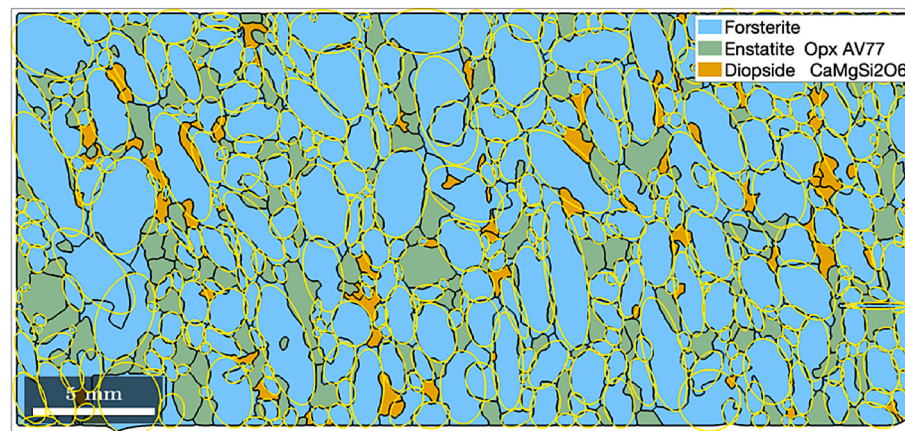


Fig. 5. EBSD map showing the 2D shapes and orientations of mineral grains of forsterite, enstatite, and diopside. Yellow ellipses are fitted to the grain areas of forsterite. EBSD data are imported and plotted using the MTEX commands. The rock sample is cpx-poor lherzolite, which is a spinel peridotite xenolith hosted by Cenozoic alkali basaltic rocks from the Tok volcanic field in SE Siberia (Tommasi et al., 2008).

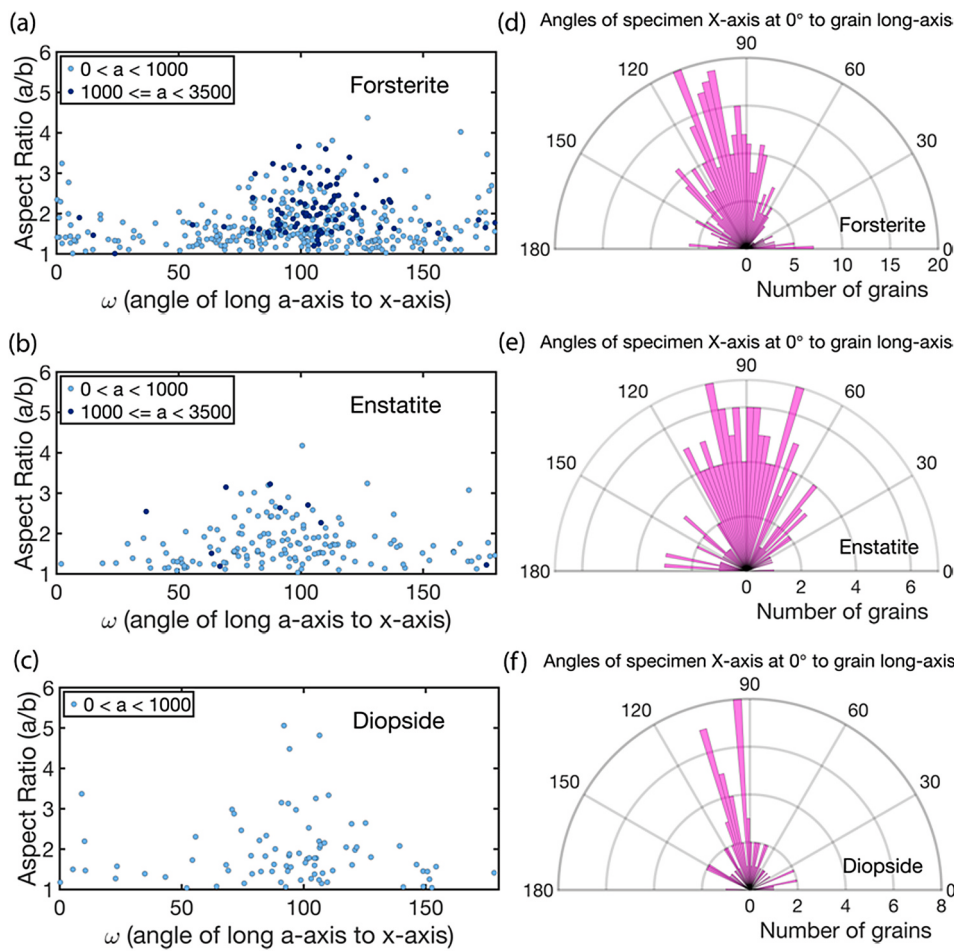


Fig. 6. Grain shapes and orientations of forsterite, enstatite, and diopside analyzed from EBSD data. (a-c) Grain aspect ratio (long a-axis divided by short b-axis) plotted against the angle of the long axis to the specimen X-axis (ω). (d-f) Polar histograms for the angles of the specimen X-axis at 0° to the long axis of grains. The rock sample is cpx-poor lherzolite from the Tok volcanic field in SE Siberia (Tommasi et al., 2008).

4.1.2. Step 2: Using the AnisEulerSC-Inputs program

We use the AnisEulerSC-Inputs program to generate a data file (*.mat) that contains all of the input parameters required to run the AnisEulerSC program. As shown in Fig. 1, we set up a MATLAB path and a title for generating the output file. The SC scheme (Willis, 1977), its initial value of the Voigt (1928) average, and the information of Euler files from EBSD data are also set in the Setup tab (Fig. 1). Based on the EBSD data analyses (described in Section 4.1.1), we specify the composition and volume fractions of minerals (83% forsterite, 14% enstatite, and 3% diopside) as well as the density, crystal symmetry, and single-crystal elastic stiffness of each mineral in the Single-crystal properties tab (Fig. 2). In the Grain shapes and orientations tab, we specify the Euler data file (*.txt) as well as the grain shapes and orientations (Fig. 3). To explore the effects of grain shapes and orientations, we first make a background SC (bgSC) model in which only the crystal orientation is considered for the spherical grains. We set the semi-axes A1, A2, and A3 of spherical grains parallel to the crystal elastic tensor axes X1, X2, and X3, respectively (Fig. 3). In this case, the grain orientation is the same as the crystal orientation. After specifying, checking, and saving the required information, a data file (*.mat) is generated, and it can be used as input data for the AnisEulerSC program.

4.1.3. Step 3: Running the AnisEulerSC program

We provide the AnisEulerSC program as a script (AnisEulerSC.m). To run the program, only the data file (*.mat) generated using the AnisEulerSC-Inputs (described in Section 4.1.2) is required. The AnisEulerSC program automatically calculates the Voigt, Reuss, and VRH

averages for each mineral and then calculates the average over all minerals. One of these simple averages, the Voigt average in this study, is used as an initial SC value. After SC iterations for convergence, the final SC model is determined. The AnisEulerSC program generates the output files of effective elastic properties and automatically plots the anisotropic seismic velocities (e.g., bgSC model in Figs. 7a and 8a).

4.2. SC modeling of anisotropic seismic properties of cracked materials

4.2.1. Background medium

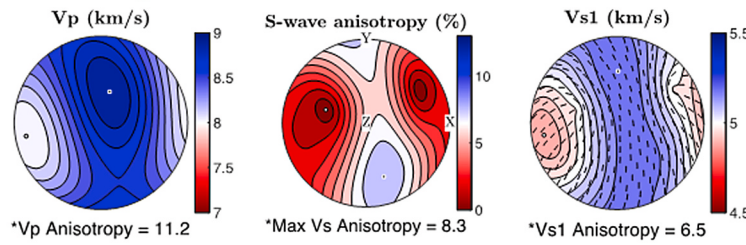
To investigate the effects of aligned cracks on the anisotropic seismic properties of a polycrystalline aggregate, we make several SC models with different shapes and orientations of aligned cracks. For background medium with no cracks, we use the bgSC model described in Section 4.1 (Figs. 7a and 8a). In the AnisEulerSC-Inputs program, we specify the elastic properties of the bgSC aggregate as the first phase. We set the bgSC aggregate to have a single orientation by specifying the Euler data file as ‘Single_orientation.txt’ in the AnisEulerSC-Inputs program (for details see Section 2.4 of the user guide). The text file is also provided with the example data.

4.2.2. Crack inclusions with ellipsoidal shapes and orientations

For the crack inclusion, we specify the Euler data file as ‘Single_orientation.txt’ for the bgSC aggregate in the AnisEulerSC-Inputs program. We assume that the ellipsoid semi-axes of cracks are parallel to the specimen axes (A1//X, A2//Y, A3//Z) and then apply the user-defined orientation in the AnisEulerSC-Inputs program. We first construct

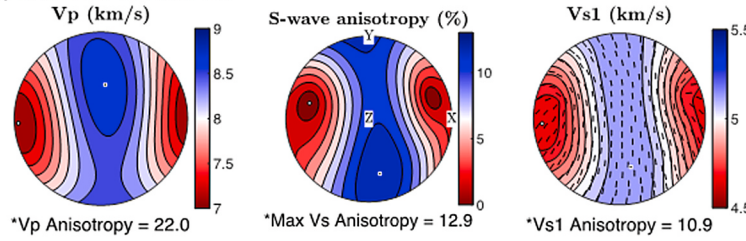
SC aggregate with no cracks

(a) Model: bgSC

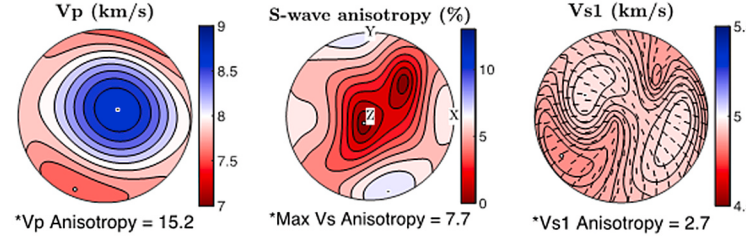


SC aggregate + 2% crack porosity

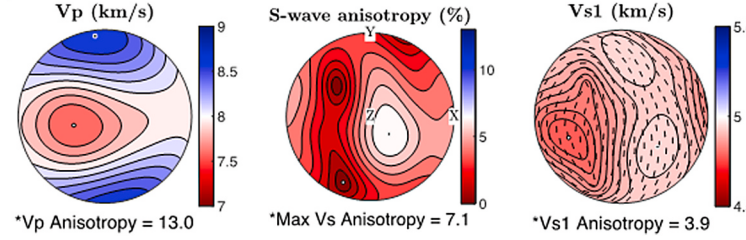
(b) Model: crackSC1



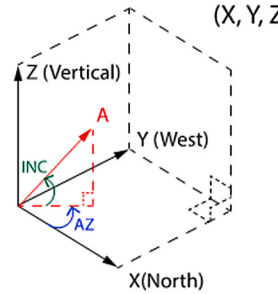
(c) Model: crackSC2



(d) Model: crackSC3



(e) Specimen reference frame (X, Y, Z)



Crack orientation

(a1:a2:a3 = 10:10:1)

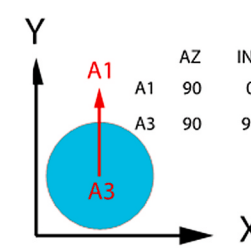
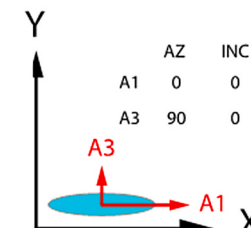
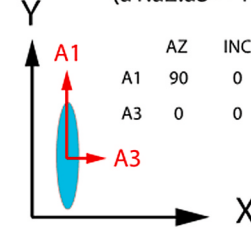


Fig. 7. Effects of the aligned cracks on the anisotropic seismic velocities. P-wave velocity (V_p , km/s), S-wave anisotropy (%), and fast S-wave velocity (V_{s1} , km/s) of the SC models are shown. (a) bgSC is composed of 83% forsterite, 14% enstatite, and 3% diopside and has spherical grains; (b) crackSC1 is composed of 98% bgSC and 2% ellipsoidal cracks (cyan ellipsoid) with symmetry axis A3 parallel to the X-axis; (c) crackSC2 is composed of 98% bgSC and 2% ellipsoidal cracks with symmetry axis A3 parallel to the Y-axis; and (d) crackSC3 is composed of 98% bgSC and 2% ellipsoidal cracks with symmetry axis A3 parallel to the Z-axis. Ellipsoid semi-axes lengths are $a_1:a_2:a_3 = 10:10:1$ for all grains. (e) The specimen reference frame for defining the crack orientations using the azimuth (AZ) and inclination (INC) of semi-axes A1 and A3. The anisotropic seismic velocities are automatically calculated and plotted using MTEX commands in the AnisEulerSC program.

three SC models: (i) crackSC1, which has oriented cracks with the short semi-axis A3 parallel to the specimen X-axis ($A_1//Y$, $A_2//Z$, and $A_3//X$; Figs. 7b and 8b); (ii) crackSC2, which has oriented cracks with the short semi-axis A3 parallel to the Y-axis ($A_1//X$, $A_2//Z$, and $A_3//Y$; Figs. 7c and 8c); and (iii) crackSC3, which has oriented cracks with the short semi-axis A3 parallel to the Z-axis ($A_1//Y$, $A_2//X$, and $A_3//Z$; Figs. 7d and 8d). The orientation of cracks is set by specifying the azimuth (AZ) from the X-axis on the XY plane and the inclination (INC) from the XY plane to the vertical Z-axis direction for semi-axes A1 and A3 (Figs. 7e and 8e) in the AnisEulerSC-Inputs program (for details see Section 2.4 of the user guide). We note that A1 should be 90° to A3 and thus A2 is automatically determined by $A_3 \times A_1$. For all SC models, we assume a

crack porosity of 2%, and all ellipsoidal crack semi-axis lengths of $a_1:a_2:a_3 = 10:10:1$ (Figs. 7b-d and 8b-d). Next, we make additional SC models with the crack shapes of $a_1:a_2:a_3 = 1:1:1$, $2:2:1$, and $5:5:1$ for each orientation (Figs. 9 and 10). In the AnisEulerSC program, the user-defined orientation can be set as a single orientation. To consider cracks with different orientations, the users must define several types of cracks with each orientation. For example, if cracks have two different orientations in a composite, crack1 and crack2 can be assumed to be different inclusions. The users have to define a single orientation for crack1 and crack2, respectively (e.g., Morales et al., 2018).

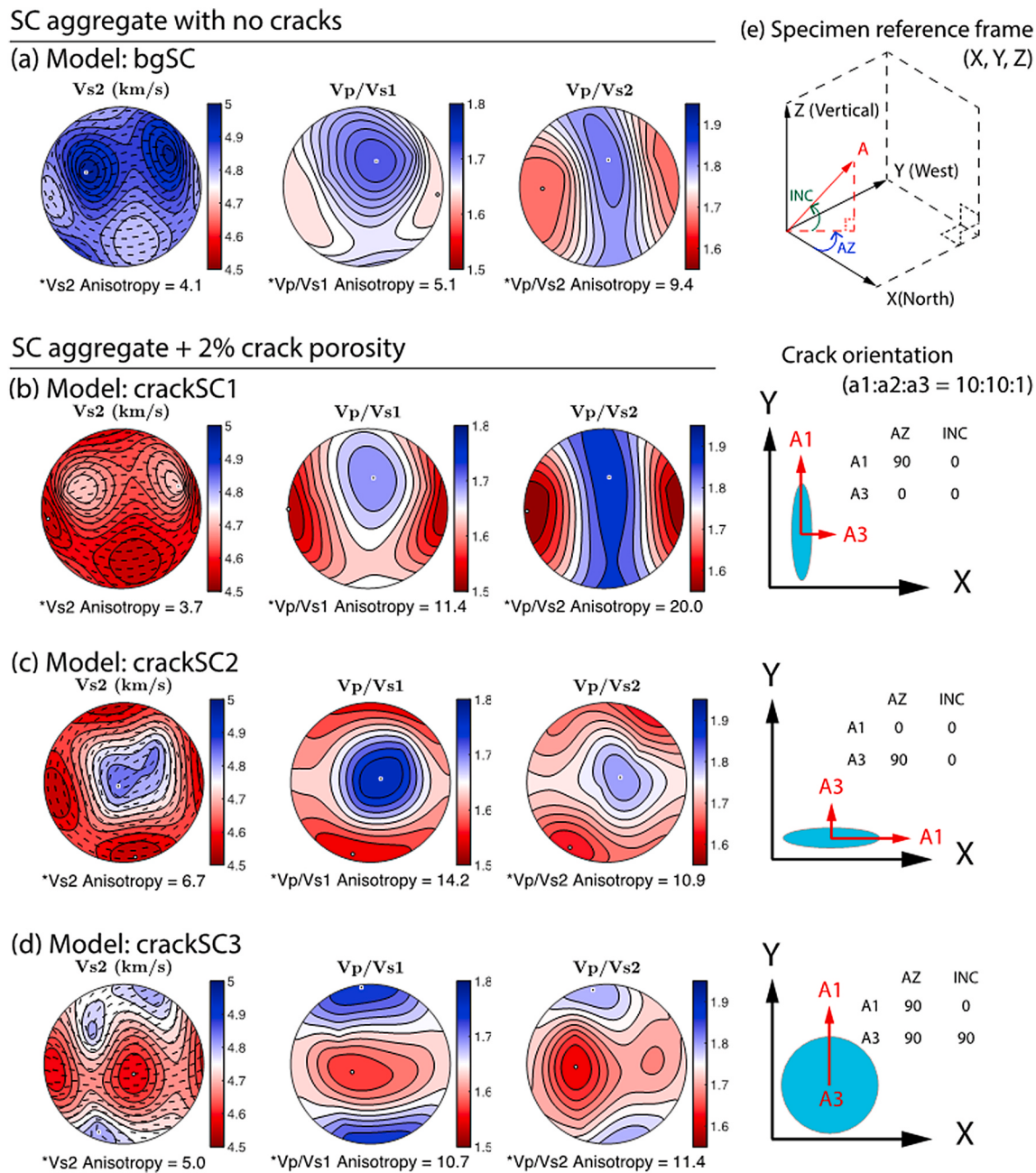


Fig. 8. Effects of the aligned cracks on the anisotropic seismic velocities. The slow S-wave velocity (V_{s2} , km/s), V_p to V_{s1} ratio (V_p/V_{s1}), and V_p to V_{s2} ratio (V_p/V_{s2}) are shown. See the caption of Fig. 7 for detailed information.

4.2.3. SC models with ellipsoidal cracks

To investigate the effects of crack orientations, we compare the anisotropic seismic velocities of the cracked SC models with that of the bgSC model. The V_p distribution of crackSC1 is similar to that of the bgSC model, but the V_p anisotropy is higher because the symmetry axis of cracks is parallel to the X-axis, which is close to the slow V_p direction of bgSC (Fig. 7b). As the symmetry axis of aligned cracks changes from the X-axis to the Y-axis (crackSC2) or the Z-axis (crackSC3), the V_p distribution changes significantly (Fig. 7c and d). The distributions of S-wave anisotropy, V_{s1} , V_{s2} , V_p/V_{s1} , and V_p/V_{s2} also show similar trends with V_p according to the symmetry axis of cracks (Figs. 7b-d and 8b-d). These results indicate that the effects of aligned cracks depend on how the anisotropic properties resultant from the preferred orientation of cracks are different from the anisotropic characteristics of the background medium.

Compared to the spherical cracks ($a_1:a_2:a_3 = 1:1:1$; Figs. 9a and 10a), ellipsoidal cracks with the symmetry axis A3 parallel to the X-axis do not change the V_p distribution (Fig. 9b-d) or the S-wave anisotropy distribution (Fig. 10b-d). However, the V_p anisotropy (Fig. 9b-d) and the maximum V_s anisotropy (Fig. 10b-d) are increased, because the long and short dimensions of cracks correspond to the fast and slow V_p axes of bgSC, respectively. As the symmetry axis A3 of cracks changes to the direction parallel to the Y-axis (Figs. 9e-g and 10e-g) and then the Z-axis (Figs. 9h-j and 10h-j), the distributions of V_p and S-wave anisotropy change significantly according to the crack shape. However, the increases in V_p anisotropy and maximum S-wave anisotropy are smaller than in the case of the symmetry axis A3 parallel to the X-axis (Figs. 9 and 10).

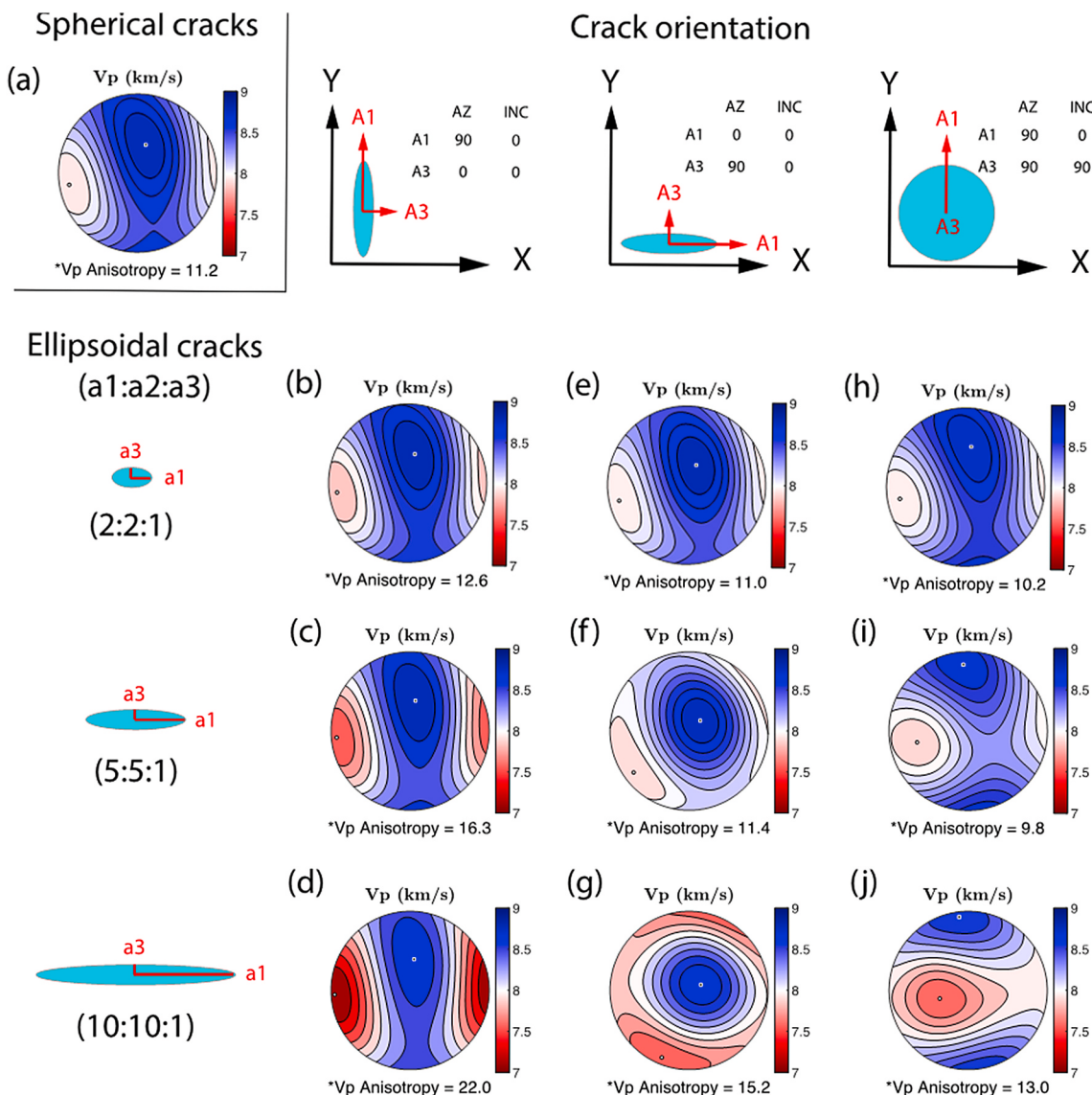


Fig. 9. P-wave velocity (V_p , km/s) variation according to the crack shapes and orientations. (a) Spherical cracks with semi-axes lengths $a_1:a_2:a_3 = 1:1:1$, (b–d) ellipsoidal cracks with symmetry axis A_3 parallel to the X-axis, (e–g) ellipsoidal cracks with symmetry axis A_3 parallel to the Y-axis, and (h–j) ellipsoidal cracks with symmetry axis A_3 parallel to the Z-axis for the semi-axes lengths $a_1:a_2:a_3 = 2:2:1$, 5:5:1, and 10:10:1. For all SC modeling, the AnisEulerSC program is used. The anisotropic seismic velocities are automatically calculated and plotted using MTEX commands in the AnisEulerSC program.

5. Discussion

5.1. Comparison of SC aggregates with simple averages

Experimentally measured velocities of elastic waves in deformed rock samples cannot be explained by the CPO alone (e.g., Burlini and Kunze, 2000; Morales et al., 2018). Burlini and Kunze (2000) investigated a calcite mylonite and concluded that the V_p anisotropy predicted from simple averages of 2.6% could not explain the measured V_p anisotropy of 5%. They attributed this result to the strong SPO of the calcite and the preferred alignment of accessory minerals along calcite grain boundaries. Morales et al. (2018) investigated antigorite-bearing rocks of serpentinite samples and concluded that CPO-based seismic velocities from simple averaging methods only matched 1/3 of the experimental velocities. However, using the crack porosity of 1.63% and assuming two crack orientations based on experimental measurements, they showed that all of the experimental velocities matched the SC models. Therefore, the CPO-derived velocities from the simple averaging methods cannot be directly compared to the experimental seismic

data, particularly when crack porosity is present in the foliation of the antigorite (Morales et al., 2018). Thus, the SC method is useful for predicting the seismic velocities of the antigorite-bearing rocks required for understanding the seismic properties of the mantle structure, such as the mantle wedge of subduction zones, because it uses CPO and SPO data as well as crack properties.

We compare simple averages with a series of SC aggregates modeled using various shapes and orientations of grains. For each SC aggregate, we use only one mineral, forsterite, with a grain shape with ellipsoidal semi-axes ratios of $a_1:a_2:a_3 = 1:AR:AR$, $AR:1:AR$, or $AR:AR:1$ (AR = aspect ratio). Fig. 11 shows the elastic stiffness components of a forsterite aggregate as a function of the aspect ratio of grains. The elastic constants of C_{22} , C_{33} , C_{44} , and C_{55} are perturbed as the aspect ratio of grains increases, indicating that anisotropic elastic properties depend on the grain shapes and orientations (Fig. 11). All components of the SC aggregates are comparable to those of the VRH average (Fig. 11). Thus, the VRH average is suitable for comparison with the SC aggregate.

We also calculate the effective isotropic moduli (bulk and shear modulus) of SC aggregates composed of 83% forsterite, 14% enstatite,

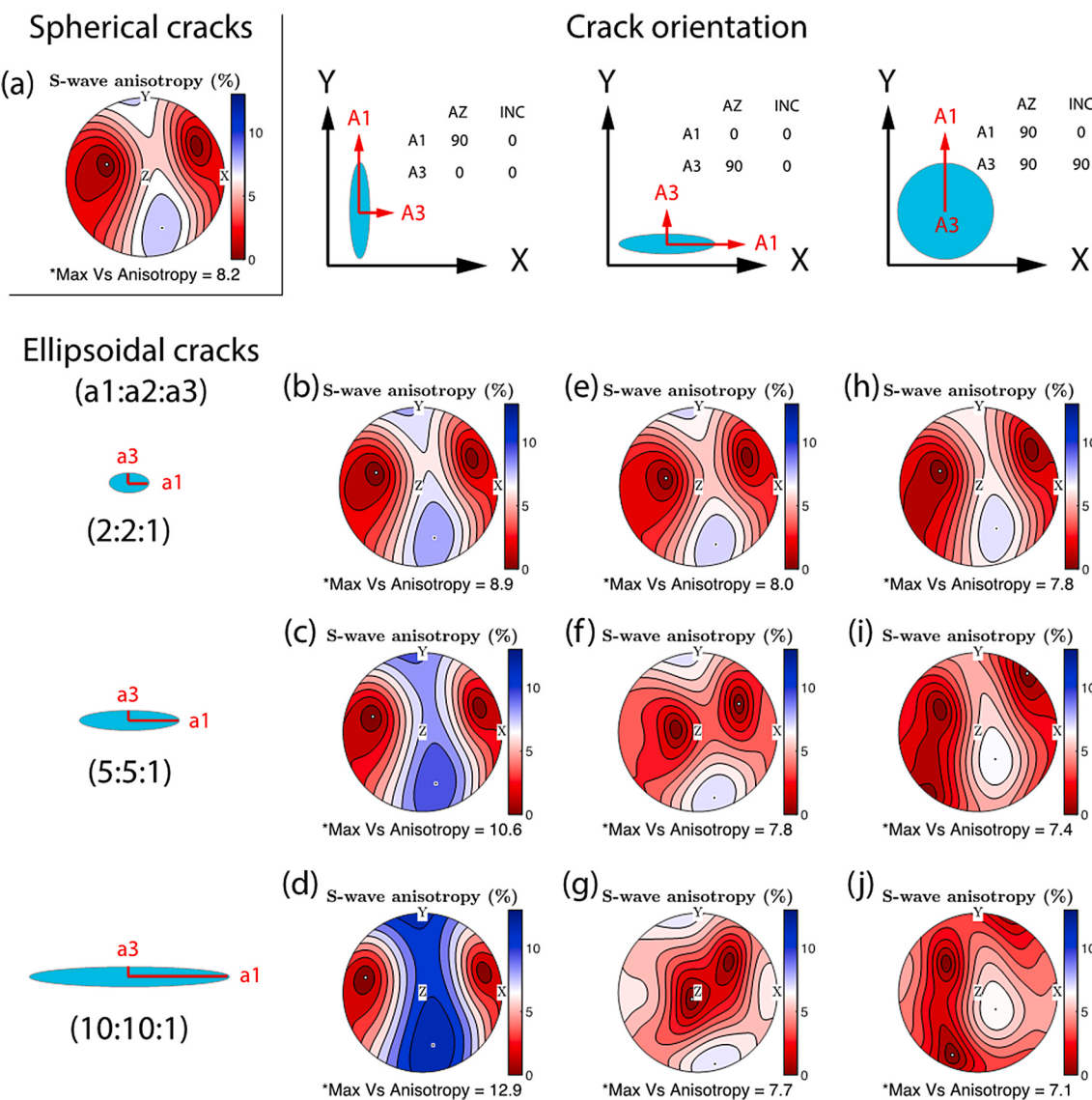


Fig. 10. S-wave anisotropy variation according to the crack shapes and orientations. See the caption of Fig. 9 for detailed information.

and 3% diopside using a numerical approach for Hashin-Shtrikman bounds (Hashin and Shtrikman, 1962, 1963) provided by Brown (2015) (Figs. 12 and 13). The bulk and shear modulus variation according to the grain shape show that the grain shape causes perturbations on the Voigt and Reuss bounds as well as the Hashin-Shtrikman bounds, although the changes are small (Fig. 12). The bulk and shear moduli variation due to the aspect ratio of grains depends on the grain orientation (Fig. 13). These results indicate that the prediction of effective elastic properties based on the anisotropic properties of minerals (e.g., grain shapes and orientations) can improve the determination of isotropic elastic moduli.

5.2. Effect of grain shape and orientation on the anisotropic elastic properties

For rocks with strong CPOs, the grain shape has a minor effect on the seismic velocities of a macroscopic polycrystalline specimen (Mainprice and Humbert, 1994). However, the grain shape can be important for materials with platy minerals, such as graphite or sheet-silicate containing rocks and aggregates with flat oriented pores (Romanowicz and Wenk, 2017). Wenk et al. (2012) showed that the P-wave anisotropy (12.6%) of a biotite gneiss sample calculated using the SC method in

which grain shapes are considered was closer to the measured P-wave anisotropy (15.3%) than the result from the SC method with no grain shapes (11.2%) considered. Morales et al. (2018) also showed that the effect of antigorite grain shape on the seismic velocities of antigorite-olivine rocks is small, but the effect on anisotropy is significant.

To investigate the effects of grain shapes and orientations on anisotropic seismic properties, we first make three SC models in which only the grain shape is different from bgSC (described in Figs. 7a and 8a). The three SC models have the grain shapes of a1:a2:a3 = 1:3:3, 3:1:3, and 3:3:1, respectively, for all minerals, and the grain orientations are the same as the crystal orientations (a1//X1, a2//X2, and a3//X3) (Fig. 14a–c). Next we make three SC models in which the grain shape of a1:a2:a3 = 3:3:1 is oriented to one of the specimen axes (Fig. 14d–f). In each SC model, all grains have the same shape. The short dimension of grain shape generally corresponds to a decrease in the elastic constant parallel to that direction. However, for a polycrystalline aggregate, it is not clear because the CPOs of minerals can also affect the overall elastic stiffness tensor. For SC models in which the ellipsoidal semi-axes of grains are parallel to the crystal elastic axes (A1//X1, A2//X2, and A3//X3), the decrease and increase in elastic constants of C₁₁, C₂₂, and C₃₃ are not directly related to the short and long dimension of grain shapes

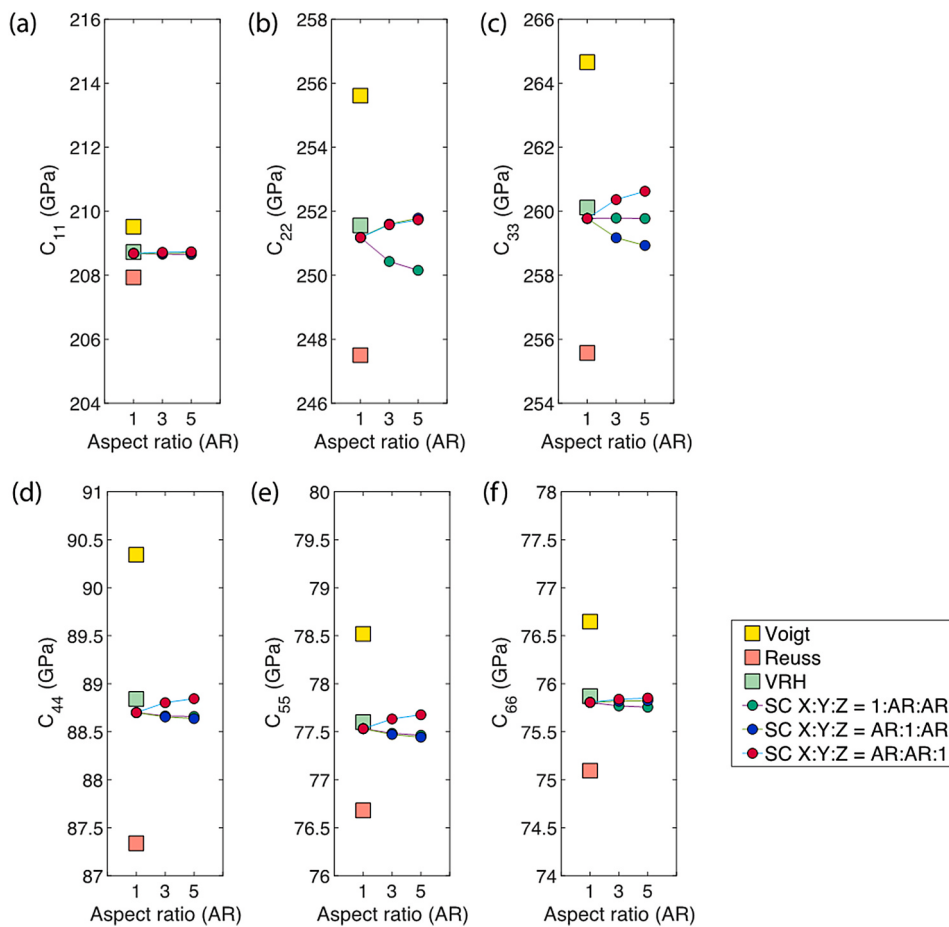


Fig. 11. Comparison of SC aggregates and simple averages. The SC aggregates are composed of only one mineral (100% forsterite with ellipsoidal grains). The ellipsoid semi-axes of grains are parallel to the crystal elastic tensor axes ($a_1//X_1$, $a_2//X_2$, and $a_3//X_3$). The shapes are $a_1:a_2:a_3 = 1:AR:AR$, $AR:1:AR$, or $AR:AR:1$ (AR = aspect ratio). The variation in elastic stiffness components of (a) C_{11} , (b) C_{22} , (c) C_{33} , (d) C_{44} , (e) C_{55} , and (f) C_{66} is plotted as a function of the aspect ratio.

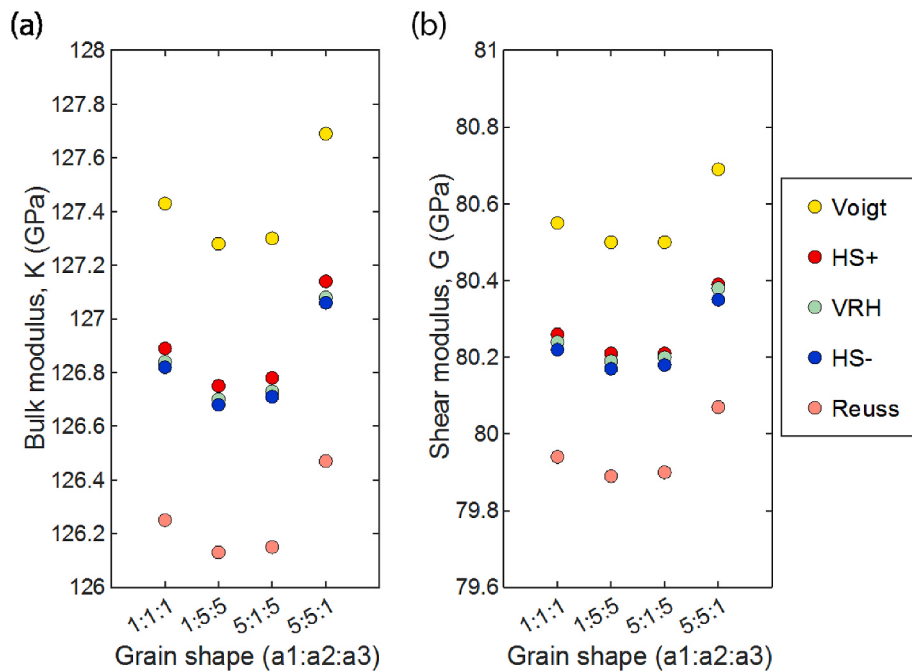


Fig. 12. Comparison of the effective isotropic moduli of SC aggregates from Hashin-Shtrikman bounds (HS+ and HS-) (Brown, 2015) with the Voigt, Reuss, and VRH averages. (a) Bulk and (b) shear modulus of four SC aggregates are calculated assuming the grain shape of $a_1:a_2:a_3 = 1:1:1$, $1:5:5$, $5:1:5$, and $5:5:1$, respectively, for all minerals. The ellipsoid semi-axes of grains are parallel to the crystal elastic tensor axes ($a_1//X_1$, $a_2//X_2$, and $a_3//X_3$). Each SC aggregate is assumed to be composed of 83% forsterite, 14% enstatite, and 3% diopside based on the EBSD data.

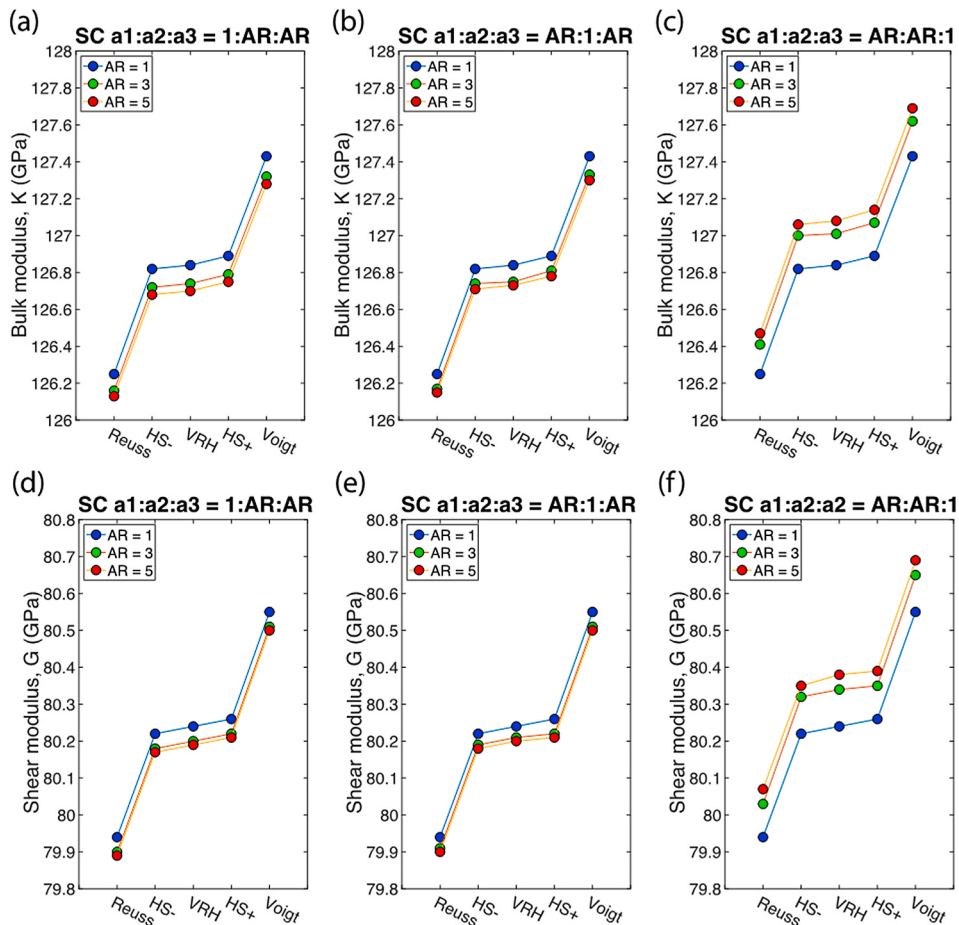
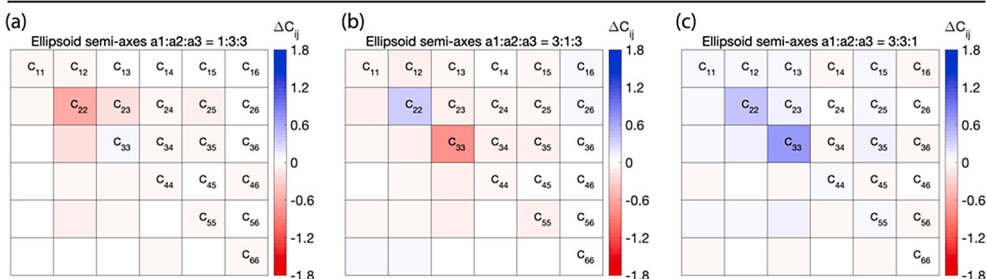


Fig. 13. Variation in effective isotropic moduli of SC aggregates according to the method for polycrystals. (a–c) Bulk and (d–f) shear modulus of Hashin-Shtrikman bounds (HS+ and HS-) (Brown, 2015) are compared to the Voigt, Reuss, and VRH averages for grain semi-axes ratios of $a_1:a_2:a_3 = 1:AR:AR$, $AR:1:AR$, and $AR:AR:1$ ($AR = \text{aspect ratio}$). The ellipsoid semi-axes of grains are parallel to the crystal elastic tensor axes ($a_1//X_1$, $a_2//X_2$, and $a_3//X_3$). Each SC aggregate is assumed to be composed of 83% forsterite, 14% enstatite, and 3% diopside and to have the same grain semi-axes ratio for all minerals.

Ellipsoid semi-axes are parallel to crystal elastic axes ($A_1//X_1$, $A_2//X_2$, $A_3//X_3$) & CPO



Ellipsoid semi-axes are parallel to specimen axes ($A_1//X$, $A_2//Y$, $A_3//Z$) & SPO

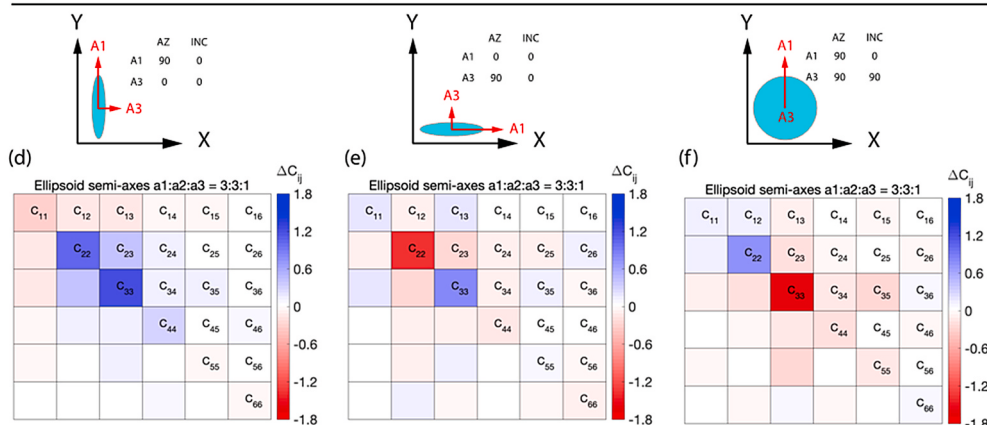


Fig. 14. Effect of grain shapes and orientations on the elastic stiffness constants C_{ij} of a polycrystalline aggregate. The change in elastic constants of SC aggregates is the difference from the bgSC model in which CPO is considered for spherical grains. (a–c) Three SC models in which grains have ellipsoid semi-axes $a_1:a_2:a_3 = 1:3:3$, $3:1:3$, and $3:3:1$, respectively, parallel to crystal elastic tensor axes ($A_1//X_1$, $A_2//X_2$, $A_3//X_3$). CPO is considered for grain orientations. (d–f) Three SC models in which ellipsoidal grains with the semi-axes $a_1:a_2:a_3 = 3:3:1$ parallel to specimen axes ($A_1//X$, $A_2//Y$, $A_3//Z$) are oriented to have the short axis A_3 parallel to the X -axis, Y -axis, and Z -axis. The orientation of grain shape is defined using the azimuth and inclination of semi-axes A_1 and A_3 .

(Fig. 14a–c). This indicates that the CPOs of minerals mainly affect the effective elastic stiffness tensor. However, for SC models in which the grains are aligned with the same orientation, it is clear that the short dimension of ellipsoidal grains corresponds to a decrease in the elastic constants parallel to that direction (Fig. 14d–f). The bgSC model with spherical grains has the elastic stiffness constants of $C_{11} < C_{22} < C_{33}$. The elastic constants of fast directions (C_{22} and C_{33}) change significantly, whereas that of the slow direction (C_{11}) changes slightly (Fig. 14d–f). This indicates that the aligned grains with ellipsoidal shapes affect the anisotropic seismic properties according to their orientation.

5.3. Effect of cracks on the anisotropic properties of a polyphase aggregate

Microcracks are important for interpreting the seismic velocities and their degree of anisotropy from experimental measurements (Matthies, 2012) because microcracks are not randomly oriented in most cases and affect the elastic anisotropy of rocks (Sayers and Kachanov, 1995). Mainprice and Humbert (1994) showed that the anisotropic elastic properties of an aggregate can change significantly because of the ellipsoidal fluid- or air-filled cracks that cause large differences in moduli between the constituents. As shown in Figs. 9 and 10, ellipsoidal cracks have a strong influence on the anisotropic seismic velocities according to the orientation of their symmetry axis. Only a 2% crack porosity is sufficient to change the seismic velocity distribution, particularly when the long axes of ellipsoidal cracks are aligned in a direction different from the fast velocity axis of a polyphase aggregate (Figs. 7–10). This is consistent with the result of differential effective medium (DEM) modeling for melt-containing rocks beneath the mid-ocean ridge by Mainprice (1997), which showed a clear change in seismic anisotropy patterns due to only 2% melt inclusions with ellipsoidal shapes.

Aligned fluid-filled cracks significantly affect seismic properties (Anderson et al., 1974). However, seismic velocities have been commonly predicted using simple averaging methods in which the shape and alignment of cracks are not considered. Ullemeyer et al. (2006) used the Voigt average to calculate the texture-related anisotropy of deformed and metamorphic rocks and compared the results to the experimentally measured P wave velocities and anisotropies. They emphasized the possibility of a fluid effect on the seismic velocity and anisotropy based on the anisotropic distributions of water-filled microcracks and pores. Baptiste et al. (2015) used the VRH average to calculate the seismic properties of mantle xenoliths based on microstructures and CPO data and compared their results to the seismological data of anisotropy measurements through the fast SKS polarization directions. Their results were used to explore the relations between deformation, melt or fluid percolation, and hydration in mantle xenoliths. However, the SC approximation may better constrain the deformation mechanisms and conditions in the lithospheric mantle than simple averages because the shape and alignment of ellipsoidal fluid-filled cracks are considered in the calculation.

5.4. Combination of SC approximation and various methods

SC approximation can be combined with other methods, such as the DEM theory, to make the effective medium of a composite. Because the SC approximation tends to overestimate crack interactions at high concentrations of inclusions compared to DEM theory, in which no interaction between inclusions is assumed (e.g., Bruner, 1976; Henyey and Pomphrey, 1982), combined SC approximation/DEM theory has been used to make an anisotropic fluid-solid composite, which is generally composed of several minerals (e.g., Hornby et al., 1994; Jakobsen et al., 2000). As most of rock microstructures are complex, combinations of several methods have been used commonly (Almqvist and Mainprice, 2017). Hornby et al. (1994) combined SC approximation with DEM theory to predict the anisotropic elastic properties of a composite composed of percolating fluid and solid phases. Le Ravalec and

Guéguen (1996) used the combination of the extended differential, SC models, and the Gassmann (1951) equation to predict the high- and low-frequency effective moduli of a saturated rock with pores or cracks. Mainprice (1997) combined DEM with Gassmann's (1951) poroelastic relationship to predict the anisotropic seismic velocities and attenuation of rocks with an anisotropic background medium with CPO and oriented melt-filled inclusions. Matthies (2012) used the GEO-MIX-SELF algorithm (Matthies, 2010), which combines elements of the SC algorithms and of the geometric mean approximation, for rocks composed of polycrystalline phases with nonspherical grain shapes and preferred orientations as well as microcracks. Huot and Singh (2018) modeled a background matrix of sediments using the SC approximation and then used it as an input for the DEM method together with either methane or seawater inclusions to predict P-wave velocity as a function of porosity. Kim et al. (2019) also modeled antigorite-olivine aggregates with crack porosity using the SC approximation and then used a background medium of the DEM method with either melt or water inclusions. They also presented a MATLAB program "GassDem" that can be used to predict the anisotropic seismic velocities and attenuation of a porous medium from microstructure using DEM theory and the poroelastic relationship of Gassmann (1951). As shown by Morales et al. (2018), the SC model can explain the experimental velocities better than simple averages such as the Voigt, Reuss, and VRH averages. Because the SC method calculates the macroscopic elastic properties based on the shape and orientation of constituents as well as the CPO of minerals, it is an essential method for the prediction of anisotropic elastic properties.

6. Conclusions

We present a MATLAB-based software, AnisEulerSC, for modeling the anisotropic seismic properties of a polycrystalline aggregate with microcracks using the SC approximation. This program utilizes the MTEX commands for texture analyses of rock samples from experimental measurements. We provide various SC models to explore the effects of grain shapes and the effects of crack shapes and orientations on the anisotropic seismic properties of a polycrystalline aggregate. These SC models show that grain shape can be an important factor controlling the anisotropic elasticity of a polycrystalline aggregate attributable to the mineral characteristics and that only a 2% crack porosity is sufficient to change the anisotropic seismic properties, although seismic velocities and their degree of anisotropy depend on the crack shape and orientation.

Authorship statement

Eunyoung Kim translated the AnisEulerSC FORTRAN77 code into a MATLAB program, performed various tests of the code and models, analyzed the results of tests, and wrote and reviewed the manuscript. Current address: Korea Institute of Geoscience and Mineral Resources, Daejeon, 34132, Republic of Korea. YoungHee Kim contributed to the interpretation of test results and reviewed the manuscript. David Mainprice wrote the original AnisEulerSC code in FORTRAN77, explained the functions of FORTRAN77 subroutines, helped in documentation of functions and demonstration of MTEX commands in the code, contributed to the interpretation of test results, and reviewed the manuscript.

Computer code availability

The source code, example input data, and user guide are available at <https://github.com/ekim1419/AnisEulerSC>.

Declaration of competing interest

The authors declare that they have no known competing financial interests or personal relationships that could have appeared to influence

the work reported in this paper.

Acknowledgments

We thank Dario Grana (Editor), Leonardo Azevedo (Associate Editor), Bjarne Almqvist, and two anonymous reviewers for their constructive comments, which improved this manuscript. This work was supported by the Creative-Pioneering Researchers Program through Seoul National University (SNU) (SNU SRnD 3345–20160014) and by the Nuclear Safety Research Program through the Korea Foundation of Nuclear Safety (KoFONS), granted financial resource from the Nuclear Safety and Security Commission (NSSC), Republic of Korea (No. 1705010).

References

- Almqvist, B.S.G., Mainprice, D., 2017. Seismic properties and anisotropy of the continental crust: predictions based on mineral texture and rock microstructure. *Rev. Geophys.* 55 (2), 367–433. <https://doi.org/10.1002/2016RG000552>.
- Anderson, D.L., Minster, B., Cole, D., 1974. The effect of oriented cracks on seismic velocities. *J. Geophys. Res.* 79 (26), 4011–4015. <https://doi.org/10.1029/JB079i026p04011>.
- Baptiste, V., Tommasi, A., Vauchez, A., Demouchy, S., Rudnick, R.L., 2015. Deformation, hydration, and anisotropy of the lithospheric mantle in an active rift: constraints from mantle xenoliths from the North Tanzanian Divergence of the East African Rift. *Tectonophysics* 639, 34–55. <https://doi.org/10.1016/j.tecto.2014.11.011>.
- Berge, P.A., Berryman, J.G., Bonner, B.P., 1993. Influence of microstructure on rock elastic properties. *Geophys. Res. Lett.* 20 (23), 2619–2622. <https://doi.org/10.1029/93GL03131>.
- Berryman, J.G., 1995. Mixture theories for rock properties. In: Ahrens, Thomas J. (Ed.), *A Handbook of Physical Constants*. American Geophysical Union, pp. 205–228. <https://doi.org/10.1029/RF003p0205>.
- Berryman, J.G., Berge, P.A., 1993. Rock elastic properties: dependence on microstructure. Symposium on Homogenization and Constitutive Modeling for Heterogeneous Materials, University of Virginia. In: Proceedings of the Symposium on Homogenization and Constitutive Modeling for Heterogeneous Materials. American Society of Mechanical Engineers - Applied Mechanics Division, Charlottesville, Virginia, pp. 1–13.
- Brown, J.M., 2015. Determination of Hashin-Shtrikman bounds on the isotropic effective elastic moduli of polycrystals of any symmetry. *Comput. Geosci.* 80, 95–99. <https://doi.org/10.1016/j.cageo.2015.03.009>.
- Bruner, W.M., 1976. Comment on ‘Seismic velocities in dry and saturated cracked solids’ by Richard J. O’Connell and Bernard Budiansky. *J. Geophys. Res.* 81 (14), 2573–2576. <https://doi.org/10.1029/JB081i014p02573>.
- Budiansky, B., 1965. On the elastic moduli of some heterogeneous materials. *J. Mech. Phys. Solid.* 13 (4), 223–227. [https://doi.org/10.1016/0022-5096\(65\)90011-6](https://doi.org/10.1016/0022-5096(65)90011-6).
- Budiansky, B., O’Connell, R.J., 1976. Elastic moduli of a cracked solid. *Int. J. Solid Struct.* 12 (2), 81–97. [https://doi.org/10.1016/0020-7683\(76\)90044-5](https://doi.org/10.1016/0020-7683(76)90044-5).
- Burlini, L., Kunze, K., 2000. Fabric and seismic properties of carrara marble mylonite. *Phys. Chem. Earth Solid Earth Geodes.* 25 (2), 133–139. [https://doi.org/10.1016/S1464-1895\(00\)00022-3](https://doi.org/10.1016/S1464-1895(00)00022-3).
- Chai, M., Brown, J.M., Slutsky, L.J., 1997. The elastic constants of an aluminous orthopyroxene to 12.5 GPa. *J. Geophys. Res.: Solid Earth* 102 (B7), 14779–14785. <https://doi.org/10.1029/97JB00893>.
- Christoffel, E.B., 1877. Ueber die Fortpflanzung von Stößen durch elastische feste Körper. *Ann. Mat. Pura Appl.* 8 (1), 193–243. <https://doi.org/10.1007/BF02420789>, 1867–1897.
- Cyprich, D., Piazolo, S., Almqvist, B.S.G., 2017. Seismic anisotropy from compositional banding in granulites from the deep magmatic arc of Fiordland, New Zealand. *Earth Planet Sci. Lett.* 477, 156–167. <https://doi.org/10.1016/j.epsl.2017.08.017>.
- Eshelby, J.D., 1957. The determination of the elastic field of an ellipsoidal inclusion, and related problems. *Proc. Roy. Soc. Lond. Math. Phys. Sci.* 241 (1226), 376.
- Gassmann, F., 1951. Über die Elastizität poröser medien. *Vierteljahrsschrift der Naturforschenden Gesellschaft in Zürich* 96, pp. 1–23 (Paper translation at: <http://sepwww.stanford.edu/sep/berryman/PS/gassmann.pdf>).
- Hashin, Z., Shtrikman, S., 1962. A variational approach to the theory of the elastic behaviour of polycrystals. *J. Mech. Phys. Solid.* 10 (4), 343–352. [https://doi.org/10.1016/0022-5096\(62\)90005-4](https://doi.org/10.1016/0022-5096(62)90005-4).
- Hashin, Z., Shtrikman, S., 1963. A variational approach to the elastic behavior of multiphase materials. *Journal Mechanics Physical Solids* 11, 127–140.
- Heney, F.S., Pomphrey, N., 1982. Self-consistent elastic moduli of a cracked solid. *Geophys. Res. Lett.* 9 (8), 903–906. <https://doi.org/10.1029/GL009i008p00903>.
- Hershey, A.V., 1954. The elasticity of an isotropic aggregate of anisotropic cubic crystals. *Journal of Applied mechanics-transactions of the ASME* 21 (3), 236–240.
- Hielscher, R., Schaeben, H., 2008. A novel pole figure inversion method: specification of the MTEX algorithm. *J. Appl. Crystallogr.* 41 (6), 1024–1037. <https://doi.org/10.1107/S0021889808030112>.
- Hill, R., 1952. The elastic behaviour of a crystalline aggregate. *Proc. Phys. Soc.* 65 (5), 349.
- Hill, R., 1965. A self-consistent mechanics of composite materials. *J. Mech. Phys. Solid.* 13 (4), 213–222. [https://doi.org/10.1016/0022-5096\(65\)90010-4](https://doi.org/10.1016/0022-5096(65)90010-4).
- Hornby, B.E., Schwartz, L.M., Hudson, J.A., 1994. Anisotropic effective-medium modeling of the elastic properties of shales. *Geophysics* 59 (10), 1570–1583. <https://doi.org/10.1190/1.1443546>.
- Huot, G., Singh, S.C., 2018. Seismic evidence for fluid/gas beneath the mentawai fore-arc basin, central sumatra. *J. Geophys. Res.* 123 (2), 957–976. <https://doi.org/10.1002/2017JB014849>.
- Isaak, D.G., Anderson, O.L., Goto, T., Suzuki, I., 1989. Elasticity of single-crystal forsterite measured to 1700 K. *J. Geophys. Res.* 94 (B5), 5895–5906. <https://doi.org/10.1029/JB094iB05p05895>.
- Isaak, D.G., Ohno, I., Lee, P.C., 2006. The elastic constants of monoclinic single-crystal chrome-diopside to 1,300 K. *Phys. Chem. Miner.* 32 (10), 691–699. <https://doi.org/10.1007/s00269-005-0047-9>.
- Jakobsen, M., Hudson, J.A., Minshull, T.A., Singh, S.C., 2000. Elastic properties of hydrate-bearing sediments using effective medium theory. *J. Geophys. Res.* 105 (B1), 561–577. <https://doi.org/10.1029/1999JB900190>.
- Kern, H., Ivankina, T.I., Nikitin, A.N., Lokajíček, T., Pros, Z., 2008. The effect of oriented microcracks and crystallographic and shape preferred orientation on bulk elastic anisotropy of a foliated biotite gneiss from Outokumpu. *Tectonophysics* 457 (3), 143–149. <https://doi.org/10.1016/j.tecto.2008.06.015>.
- Kim, E., Kim, Y., Mainprice, D., 2019. GassDem: a MATLAB program for modeling the anisotropic seismic properties of porous medium using differential effective medium theory and Gassmann’s poroelastic relationship. *Comput. Geosci.* 126, 131–141. <https://doi.org/10.1016/j.cageo.2019.02.008>.
- Kinoshita, N., Mura, T., 1971. Elastic fields of inclusions in anisotropic media. *Phys. Status Solidi* 5 (3), 759–768. <https://doi.org/10.1002/pssa.2210050332>.
- Kröner, E., 1958. Computation of the elastic constants of polycrystals from constants of single crystals. *Z. Phys.* 151, 504–518.
- Le Ravalec, M., Guéguen, Y., 1996. High- and low-frequency elastic moduli for a saturated porous/cracked rock-Differential self-consistent and poroelastic theories. *Geophysics* 61 (4), 1080–1094. <https://doi.org/10.1190/1.1444029>.
- Mainprice, D., 1990. A FORTRAN program to calculate seismic anisotropy from the lattice preferred orientation of minerals. *Comput. Geosci.* 16 (3), 385–393. [https://doi.org/10.1016/0098-3004\(90\)90072-2](https://doi.org/10.1016/0098-3004(90)90072-2).
- Mainprice, D., 1997. Modelling the anisotropic seismic properties of partially molten rocks found at mid-ocean ridges. *Tectonophysics* 279 (1), 161–179. [https://doi.org/10.1016/S0040-1951\(97\)00122-4](https://doi.org/10.1016/S0040-1951(97)00122-4).
- Mainprice, D., 2007. Seismic anisotropy of the deep Earth from a mineral and rock physics perspective. In: Schubert, G. (Ed.), *Treatise on Geophysics*. Elsevier, pp. 437–492. <https://doi.org/10.1016/B978-044452748-6.00045-6>.
- Mainprice, D., Hielscher, R., Schaeben, H., 2011. Calculating anisotropic physical properties from texture data using the MTEX open-source package. *Geological Society, London, Special Publications* 360 (1), 175. <https://doi.org/10.1144/SP360.10>.
- Mainprice, D., Humbert, M., 1994. Methods of calculating petrophysical properties from lattice preferred orientation data. *Surv. Geophys.* 15 (5), 575–592. <https://doi.org/10.1007/BF00690175>.
- Matthies, S., 2010. On the combination of self-consistent and geometric mean elements for the calculation of the elastic properties of textured multi-phase samples. *Solid State Phenom.* 160, 87–93. <https://doi.org/10.4028/www.scientific.net/SSP.160.87>.
- Matthies, S., 2012. GEO-MIX-SELF calculations of the elastic properties of a textured graphite sample at different hydrostatic pressures. *J. Appl. Crystallogr.* 45 (1), 1–16. <https://doi.org/10.1107/S002188981104338X>.
- Morales, L.F.G., Mainprice, D., Kern, H., 2018. Olivine-antigorite orientation relationships: microstructures, phase boundary misorientations and the effect of cracks in the seismic properties of serpentinites. *Tectonophysics* 724–725, 93–115. <https://doi.org/10.1016/j.tecto.2017.12.009>.
- Mura, T., 1987. *Micromechanics of Defects in Solids*, Second. Martinus Nijhoff, Dordrecht, The Netherlands. <https://doi.org/10.1007/978-94-009-3489-4>.
- Reuss, A., 1929. Berechnung der Fließgrenze von Mischkristallen auf Grund der Plastizitätsbedingung für Einkristalle. *J. Appl. Math. Mech.* 9 (1), 49–58. <https://doi.org/10.1002/zamm.19290090104>.
- Romanowicz, B., Wenk, H.-R., 2017. Anisotropy in the deep earth. *Phys. Earth Planet. Sci.* 269, 58–90. <https://doi.org/10.1016/j.pepi.2017.05.005>.
- Sayers, C.M., Kachanov, M., 1995. Microcrack-induced elastic wave anisotropy of brittle rocks. *J. Geophys. Res.* 100 (B3), 4149–4156. <https://doi.org/10.1029/94JB03134>.
- Sayers, C.M., Munster, J.G., 1991. Microcrack-induced seismic anisotropy of sedimentary rocks. *J. Geophys. Res.: Solid Earth* 96 (B10), 16529–16533. <https://doi.org/10.1029/91JB01232>.
- Simmons, G., Richter, D., 1976. Microcracks in rocks. In: Strens, R.G.J. (Ed.), *The Physics and Chemistry of Minerals and Rocks*. John Wiley & Sons Ltd., pp. 105–137.
- Stiller, H., Wagner, F.C., Vollständig, H., 1977. A two-phase model for the description of the influence of cracks on the P- and S-wave velocities in dry and saturated rock samples. *Tectonophysics* 43 (3), 181–197. [https://doi.org/10.1016/0040-1951\(77\)90116-0](https://doi.org/10.1016/0040-1951(77)90116-0).
- Tommasi, A., Vauchez, A., Ionov, D.A., 2008. Deformation, static recrystallization, and reactive melt transport in shallow subcontinental mantle xenoliths (Tok Cenozoic volcanic field, SE Siberia). *Earth Planet Sci. Lett.* 272 (1), 65–77. <https://doi.org/10.1016/j.epsl.2008.04.020>.
- Ullemeyer, K., Siegesmund, S., Rasolofosaon, P.N.J., Behrmann, J.H., 2006. Experimental and texture-derived P-wave anisotropy of principal rocks from the TRANSALP traverse: an aid for the interpretation of seismic field data. *Tectonophysics* 414 (1), 97–116. <https://doi.org/10.1016/j.tecto.2005.10.024>.
- Voigt, W., 1928. *Lehrbuch der Kristallphysik*. Teubner-Verlag, Leipzig.
- Walsh, J.B., 1965a. The effect of cracks on the compressibility of rock. *J. Geophys. Res.* 70 (2), 381–389. <https://doi.org/10.1029/JZ070i002p00381>.

- Walsh, J.B., 1965b. The effect of cracks on the uniaxial elastic compression of rocks. *J. Geophys. Res.* 70 (2), 399–411. <https://doi.org/10.1029/JZ070i002p00399>.
- Wenk, H.-R., Vaslin, R.N., Kern, H., Matthies, S., Vogel, S.C., Ivankina, T.I., 2012. Revisiting elastic anisotropy of biotite gneiss from the Outokumpu scientific drill hole based on new texture measurements and texture-based velocity calculations. *Tectonophysics* 570–571, 123–134. <https://doi.org/10.1016/j.tecto.2012.06.023>.
- Willis, J.R., 1977. Bounds and self-consistent estimates for the overall properties of anisotropic composites. *J. Mech. Phys. Solid.* 25 (3), 185–202. [https://doi.org/10.1016/0022-5096\(77\)90022-9](https://doi.org/10.1016/0022-5096(77)90022-9).
- Wu, T.T., 1966. The effect of inclusion shape on the elastic moduli of a two-phase material. *Int. J. Solid Struct.* 2 (1), 1–8. [https://doi.org/10.1016/0020-7683\(66\)90002-3](https://doi.org/10.1016/0020-7683(66)90002-3).